Title

A Light Emitting Diode (LED) Based Spatial Frequency Domain Imaging System for Optimization of Photodynamic Therapy of Nonmelanoma Skin Cancer: Quantitative Reflectance Imaging

Journal

Lasers in Surgery and Medicine, 45(4)

ISSN

0196-8092

Authors

Saager, RB

Cuccia, DJ

Saggese, S

et al.

Publication Date

2013-04-01

DOI

10.1002/lsm.22139

Published in final edited form as:
Lasers Surg Med. 2013 April ; 45(4): 207–215. doi:10.1002/lsm.22139.

A Light Emitting Diode (LED) Based Spatial Frequency Domain Imaging System for Optimization of Photodynamic Therapy of Nonmelanoma Skin Cancer: Quantitative Reflectance Imaging

R. B. Saager, PhD[1], **D. J. Cuccia, PhD**[2], **S. Saggese, PhD**[2], **K. M. Kelly, MD**[3], and **A. J. Durkin, PhD**[3]

[1]Beckman Laser Institute, UC Irvine, Irvine, California

[2]Modulated Imaging, Inc, Irvine, California

[3]Beckman Laser Institute, UC Irvine, Irvine, California

Abstract

Background—Photodynamic therapy (PDT) offers the potential for enhanced treatment of nonmelanoma skin cancer (NMSC) with minimal scarring. Yet, PDT has not achieved consistent long term effectiveness to gain widespread clinical acceptance for treatment of skin cancer. Therapeutic response varies between practitioners, patients and lesions. One important contributing factor is the absence of quantitative tools to perform *in vivo* dosimetry. To this end, we have developed a new quantitative imaging device that can be used to investigate parameters related to optimizing dosimetry.

Methods—We present a spatial frequency domain imaging (SFDI) based device designed to: (1) determine the optical properties at the therapeutic wavelength, which can inform variations in light penetration depth and (2) measure the spatially resolved oxygen saturation of the skin cancer lesions and surrounding tissue. We have applied this system to a preliminary clinical study of nine skin cancer lesions.

Results—Optical properties vary greatly both spatially [101%, 48% for absorption and reduced scattering, respectively] and across patients [102%, 57%]. Blood volume maps determined using visible wavelengths (460, 525, and 630 nm) represent tissue volumes within ~1 mm in tissue (1.17 ± 0.3 mm). Here the average total hemoglobin concentration is approximately three times greater in the lesion than that detected in normal tissue, reflecting increased vasculature typically associated with tumors. Data acquired at near infrared wavelengths (730 and 850 nm) reports tissue blood concentrations and oxygenations from the underlying dermal microvasculature (volumes reaching 4.36 ± 1.32 mm into tissue).

Conclusions—SFDI can be used to quantitatively characterize *in vivo* tissue optical properties that could be useful for better informing PDT treatment parameters. Specifically, this information provides spatially resolved insight into light delivery into tissue and local tissue oxygenation, thereby providing more quantitative and controlled dosimetry specific to the lesion. Ultimately, by optimizing the execution of PDT, this instrument has the potential to positively improve treatment outcomes.

*Correspondence to: Dr. R.B. Saager, Beckman Laser Institute, 1002 Health Sciences Rd. East, Irvine, CA 92612. rsaager@uci.edu.

Conflict of Interest Disclosures: All authors have completed and submitted the ICMJE Form for Disclosure of Potential Conflicts of Interest and none were reported.

Keywords

photodynamic therapy; skin cancer; optical imaging; spectroscopy

INTRODUCTION

Nonmelanoma skin cancer (NMSC), which includes basal cell carcinoma (BCC) and squamous cell carcinoma (SCC), is the most common type of skin cancer in humans. Approximately 13 million white non-Hispanics living in the United States at the beginning of 2007 have had at least 1 NMSC [1]. While most NMSCs are treated surgically, those who suffer from Neviod basal cell carcinoma syndrome or those who are immunocompromised, including those who are organ transplant recipients can develop many, relatively large lesions at high frequency [2–4]. For these groups, standard treatments are not practical or advantageous, due to the sheer number, size, and frequency of occurrence of these lesions over a lifetime. PDT can fill an immediate and significant need within these populations. Furthermore, NMSC lesions commonly occur in cosmetically sensitive areas, including the face, for which therapies, such as PDT, that minimize scarring, are attractive [5]. Finally, for subjects already having one NMSC, there is a high probability of others developing in the surrounding tissue [6]. Given selective sensitization and destruction of diseased tissue associated with PDT, it is considered by some to be an ideal form of therapy [7].

Small studies exploiting PDT for the treatment of BCC's have shown fair success [8–11]. However, a systematic review of randomized controlled trials performed as of 2004 indicated that there was little research available to support the use of PDT for BCC; the authors concluded that there was "comparatively high recurrence rates with PDT when compared to other treatments" (e.g., relative to surgical excision, there is a 4.4× higher rate of recurrence using PDT) [12]. A recent 72 patient study, however, suggests that PDT using 5-aminolaevulinic acid provided a similarly high efficacy to that of surgery for BCC with better cosmetic outcomes [13]. Similar results have also been reported when SCCs are considered for PDT [14–16], suggesting that broad discussions of PDT efficacy in skin could be directed towards generalized NMSCs. While PDT has the potential to become an effective treatment modality, further rigorous and quantitative study is needed to isolate the causes and potentially address this inconsistent performance.

One area that has continually been cited as a high priority requirement in order for PDT to gain acceptance is the development of tools to perform *in vivo* dosimetry. Related to this, there is a simple model that indicates a relationship between the drug concentration, light exposure and tissue oxygenation where a particular photodynamic result can be achieved over a range of light/drug combinations [17]. These parameters, however, are dependent on local details of physiology and these can vary within an individual lesion and certainly between different lesions from different subjects. In the absence of *in vivo* dosimetry, the standard method to control the photodynamic dose is to specify the amount of photosensitizer applied to the tissue which is used in conjunction with a fixed light irradiance over the entire treatment area within a fixed amount of time. Under ideal circumstances this may work, but PDT studies indicate a considerable variation in the treatment response [18]. Three major sources of variation have been identified and these are likely to influence outcome. These include: (1) photosensitizer uptake variations [19], (2) tissue optical properties and tumor geometry [20], and (3) tissue oxygenation levels during treatment [21,22].

Methods for *in vivo* dosimetry for characterizing and monitoring PDT have been in development for a number of years, however, thus far, these systems have been fiber based

and thus sample only a small region of tissue, without providing detailed spatial information [23,24]. Spatial frequency domain imaging (SFDI), which is the basis of the technology presented in this paper, has the potential to provide spatially resolved dosimetry information from a lesion, and surrounding tissue. Specifically, SFDI is a method of determining the optical properties of tissue in a non-contact, reflectance geometry. SFDI has distinct advantages over other optical techniques in that it is (1) quantitative in its determination of absorption and reduced scattering as well as tissue chromophores including oxy and deoxyhemoglobin concentration and it is (2) an image based approach which allows for high resolution (~50 μm) lateral imaging at the surface of tissue, over relatively large fields of view (several to tens of cm), with the ability to detect subsurface optical properties to millimeters depth[25].

In this paper we will describe a new SFDI instrument specifically designed for quantative studies of *in vivo* skin and skin cancer. While other investigations have been published using SFDI instrumentation that either (1) use LEDs as illumination sources [26], (2) span visible and near infrared regimes [27,28], or (3) collect fluorescence images [29,30], this instrument integrates all three aspects into a single, unified imaging platform. In addition, we report results from a small scale study involving human subjects in which we demonstrate the ability to assess the spatial and inter-subject variation of optical properties at the PDT treatment wavelength from in NMSC lesions. We also illustrate the capacity to quantify spatially resolved tissue oxygenation within these lesions.

MATERIALS AND METHODS

Instrumentation and Testing

We designed and fabricated a combined quantitative imaging and PDT treatment system specifically to investigate factors that affect dosimetry. This instrument uses five different LEDs, centered at 460, 525, 630, 730, and 850 nm to provide interrogation of tissue at discrete wavelength bands, where each LED has a spectral bandwidth of 10–15 nm, full-width, half-maximum. These wavelengths have been selected to quantify the concentration of oxygenated and deoxygenated hemoglobin in both visible and near infrared wavelength regimes, described in more detail in later sections of this paper. The spatially resolved optical properties determined at 630 nm also provide insight as to how the treatment light (typically ranging from 630 to 640 nm, depending on the specific photosensitizer product used) will interact with the tissue region of interest. All light sources are computer controlled and can be sequentially projected through the imaging/treatment head of the system to illuminate a 40.5 mm × 30 mm area of tissue.

In the imaging/treatment head, a digital micromirror device (DMD; DLP developers kit, Texas Instruments) system is used to project structured patterns of light from each of the LEDs onto the tissue. Details related to how this pattern-encoded illumination approach (SFDI) can determine the optical properties of tissue will be explained in more detail in the next section. In addition to providing a source of spatially modulated illumination as is used in SFDI, the DMD is used to correct spatial variation in the light in the plane of the tissue, ensuring that the intensity of illumination is homogeneous across the field of view.

Conjugate to this image-based projection system, a CCD camera (Lm135, 12 bit Monochrome, Lumenera) is located within the imaging/treatment head (Fig. 1). This monochromatic CCD is employed as an imaging detector with a coincident image plane and field of view to that of the projected spatially modulated illumination. A polarizer/analyzer pair is placed in front of the projection and detection systems, respectively, in order to block specularly reflected light. Additionally, while not employed in this study, a long pass filter can be placed in front of the camera, enabling this imaging system to capture fluorescence as

well as tissue reflectance. We have recently published a description of a method to determine photosensitizer concentration in phantoms and in skin using fluorescence imaging and details are described in Saager et al. [31].

Custom built data acquisition software and firmware have been developed to control the LED light sources, DMD and camera. The data acquisition user interface, written in C#, enables the user to easily manipulate the selection of spatial frequencies and to control the drive current delivered to each LED.

Reflectance Image Acquisition and Data Processing

In reflectance mode, each LED is serially triggered and directed to the DMD via a fiber bundle. A sinusoidal pattern is projected at three spatially off-set phases (0°, 120°, and 240°) for each spatial frequency. This cycle is repeated for each LED.

By demodulating the three phase images for a given LED and spatial frequency, the AC component to the diffuse reflectance can be extracted. We have demonstrated that SFDI can uniquely separate absorption from reduced scattering coefficient by modeling the change in this AC component of diffuse reflectance as a function of the spatial frequency projected on the tissue [32].

The wavelengths selected for this particular instrument span both visible and near infrared regimes. Scattering dominates absorption in the near infrared regime in tissue ($\mu'_s \gg \mu_a$), which permits the use of the diffusion approximation for modeling of light transport in tissue [33]. This is not the case in the visible, where absorption and scattering are within the same order of magnitude. To this end, Monte Carlo based models have been developed to model light transport in tissue in non-diffusive regimes. For all data collected from the instrument developed here, a scaled, homogeneous Monte Carlo model was used to model the spatial frequency dependent tissue response in both visible and near infrared regimes. The performance of this Monte Carlo model approach in both visible and near infrared regimes has been demonstrated elsewhere [34].

Imaging of NMSC Lesions

NMSC lesions from eight subjects (nine lesions total) were imaged in this study, under IRB approved protocol #HS2008-6439. Under this protocol, subjects were admitted if they had either biopsy confirmed BCC or a suspect lesion that was believed to be NMSC based on clinical judgment. The latter were subsequently biopsied after being imaged by our instrument. The cohort with biopsy confirmed BCC underwent surgical removal as the size of the identified lesion was larger than that of the confirming biopsy. All lesions were ultimately confirmed as either BCC (six lesion) or SCC-*in situ* (three lesions). Table 1 summarizes the information related to the lesions that were imaged. It is worth noting that the lesion sites of this initial study were limited to the torso, back and extremities due to the ease of accessibility for the current instrument build. We acknowledge that NMSCs do also occur in regions with more complex imaging geometries, such as the head and neck. Newer instrumentation is in development that will account for these complex geometries and has recently been applied to quantitative imaging of the face [26].

Each lesion was imaged with the SFDI instrument operating in reflectance mode. This included images at all five LED wavelengths, with six spatial frequency illumination projections (ranging from 0 to 0.5 mm^{-1}), where each individual frequency was projected at three spatially shifted phases (0°, 120°, and 240°). This acquisition sequence, which is described in detail elsewhere [32], resulted in a stack of 90 images and required a total of 10–15 seconds to complete. Total acquisition times varied from subject to subject as a

consequence of the auto-exposure function of the system that was designed to optimize the dynamic range of the camera. A reference measurement of a solid tissue simulating phantom, having known optical properties was also collected at the time of measurement for instrument calibration [32].

RESULTS

Figure 2 illustrates the spatially resolved results measured at 630 nm (an example of a PDT treatment laser wavelength) from one example lesion (BCC). Though this may not be a direct comparison between imaging modalities, little contrast is evident in the dermoscopic image of the lesion (Dermlite Foto, crossed-polarized three color digital image), whereas the quantitative absorption and reduced scattering maps reveal structural heterogeneities that may significantly impact the therapeutic light transport in tissue. This will be discussed further.

Spatial and Subject Variation in Optical Properties

Table 2 summarizes the average and range of optical properties detected within the lesions imaged at 630 nm. These optical property maps were spatially filtered using a 3 × 3 pixel median filter to ensure that range of optical properties reported here are not due to any single pixel noise artifacts, but rather reflect the actual range of properties within the tissue.

In general, the average range in spatially resolved absorption coefficient values relative to the mean absorption coefficient of that specific lesion and surrounding tissue was ±101% and the reduced scattering coefficient varied spatially ±48% relative to the tissue average reduced scattering coefficient value. We refer to this as the intra-subject or spatial variability in optical property, as this captures the variability in optical properties within each lesion. When comparing the average tissue optical properties across the group of lesions measured here, there was a wide range of values recorded; absorption coefficient varied ±102% and reduced scattering coefficient varied ±57%. We refer to this variation as the inter-subject variability in optical property, as this captures the differences in the average optical properties from patient to patient.

Using the optical penetration depth metric, $\delta = (3\mu_a(\mu_a+\mu'_s))^{-1/2}$ [20] as a rough estimate for penetration of 630 nm light in tissue, we can infer how the localized optical properties of these lesions will affect the delivery of therapeutic light dose. δ is defined as a one-dimensional estimator that describes the depth in tissue at which the light fluence rate drops to 1/*e* (36.8%) of its incident fluence rate. This metric is empirically determined from the absorption coefficient, μ_a, and the reduced scattering coefficient, μ'_s. These are the same tissue optical parameters that are extracted from the SFDI measurements at each individual wavelength. Here, across all subjects, the average penetration depth is 3.27 mm with a standard deviation of ±1.19 mm, however when looking at the spatially resolved ranges, these values can vary by an order of magnitude (from 0.89 to 12 mm).

Impact of Biopsies

Ideally, we would image lesions in the absence of perturbation. However, it is typical that a biopsy is done on suspect lesions in order to confirm the diagnosis. In the course of this study we imaged several lesions that had been biopsied several weeks in advance of imaging. To that end, we were able to observe perturbations in the tissue optical properties that have the potential to alter the light dosimetry, if not addressed. Figure 3 shows the reduced scattering coefficient maps from four lesions imaged post-biopsy, overlaid by the location where the biopsies had been taken. The lesions in Figure 3, top left and right, which extended beyond the area where the biopsies were taken, indicate a distinct region of

decreased scattering that correlates with the biopsy site. This result suggests that the biopsy may cause a disruption of the dermal bed and thereby alter how the therapeutic light may travel through the tissue; in this particular case, permitting it to travel deeper into tissue. In Figure 3 (bottom left and right), however, there are distinct regions of increased scattering around the periphery of the biopsy site. This may be attributed to the proliferative phase of a wound healing response [34].

Mapping Oxygen Saturation

Figure 4 shows an example of spatially resolved total hemoglobin concentration and oxygenation from a BCC region for both visible and near infrared wavelengths. Chromophore concentrations were calculated separately for these two regimes since the optical properties vary greatly between the visible and the near infrared. In particular, in the visible wavelength regime (460, 525, and 630 nm), both reduced scattering and absorption coefficient values are much higher (~3× and 10×, respectively) in tissue than those encountered in the near infrared (730 and 850 nm) [27]. As a result, visible light does not interrogate as deeply as near infrared and the measured absorption values represent chromophores more superficially present in tissue. As expected, the overall concentration of hemoglobin is lower when calculated using data obtained from visible wavelengths, since these wavelengths access only the blood from the microvasculature near the papillary dermis, targeting primarily the properties within the lesion itself. On the other hand, near Infrared wavelengths interrogate several millimeters into tissue and thus the measured hemoglobin concentration in this wavelength range contains contributions from both the lesion and the volume of tissue underlying the lesion. Concentration values for both hemoglobin species reported from the near infrared wavelengths are in good agreement with those published in literature for blood concentration and oxygenation in skin [35].

Table 3 provides a summary of average concentration and oxygenation values from the lesions and adjacent, clinically normal tissues. When visible wavelengths are used, total blood volume determined from regions within lesions are approximately three times greater than the surrounding clinically normal tissue. This is an indication of superficial vasculature in the lesion that may be correlated with angiogenesis. Within the cohort of lesions imaged post-biopsy, the observed increase in oxygen saturation may also be due in part to wound vascularization related to healing. Total hemoglobin and oxygenation values derived from near infrared wavelengths are much more consistent, indicating that these values, in the context of superficial lesions, primarily come from the normal vasculature beneath the lesion. It is anticipated that more invasive tumors will present in the near infrared data as well. To help support this claim, the estimated penetration depth each regime of light (visible or near infrared) interrogated into tissue is included, using the same method of estimation mentioned above [20]. While the average penetration depth varied from subject to subject, in general, visible light interrogated 1.17 ± 0.3 mm into tissue and near infrared interrogated down to 4.36 ± 1.32 mm.

DISCUSSION

We have developed a quantitative imaging system to determine the optical properties of NMSC and to spectroscopically monitor tissue oxygenation supply via determination of blood and oxygen concentration in tissue microvasculature.

This study was conducted in order to validate the performance of a SFDI system and technique to characterize *in vivo* skin prior to PDT treatment. The results presented here reveal large spatially resolved heterogeneities as illustrated in Table 2, reinforcing the importance of quantitative imaging techniques like SFDI for pre-treatment planning. While the thickness of BCC lesions can range in millimeters [36], the differences in penetration

depth shown in this initial study illustrate the profound impact this variance in optical property can have on the delivery of a therapeutically effective light dose throughout the relevant volume of tissue. The most extreme variation in optical properties occurred in the subset of lesions which were imaged after biopsy, despite the fact that biopsies were done several weeks in advance of imaging. For this group, the large variability in scattering can also have direct implications to the penetration depth and dosimetry of therapeutic light. Given this result, therapeutic light penetration may be limited to only superficial tissue, particularly in the regions of high scattering associated with the proliferative granulation phase of wound healing [34]. Without *a priori* insight into the penetration depth of the therapeutic light, there is the potential for deeply embedded cancer cells to never receive sufficient light dose [37], leaving them untreated and potential viable to continue growth. Likewise, in regions where the optical properties are low, light delivery might be too high; in this case, the local oxygen supply may be depleted too quickly, resulting in the insufficient generation of oxygen radicals in effected cells.

It is worth noting that the penetration depth metric used here is based on a homogeneous model and will not account for depth resolved heterogeneities, under planar illumination conditions. This metric was employed for its simplicity to illustrate the effect of the large variance in optical properties may impart on light delivery. Full three-dimensional models of light transport and more precise metrics, such as those developed by Carp et al. [38] that corrects the penetration depth metric in non-diffuse optical regimes, to translate the spatially resolved optical property data in to rigorous, quantitative models for volumetric therapeutic light dosimetry. Also, a dedicated study of biopsied lesions would be warranted to conclusively understand the dynamics of the wound healing response in these lesions and potential impact it may have on successful PDT treatment.

The study presented here has also demonstrated the capabilities of this instrument to provide spatially resolved tissue oxygenation. This is done by carrying out using a standard least-square fit approach relying on *a priori* knowledge of the extinction coefficients of the chromo-phores that contribute to the detected signals in the visible and near infrared wavelengths ranges (i.e., oxy- and deoxy-hemoglobin as well as melanin). From the multispectral aspect of this quantitative optical instrument, it is possible to generate spatially resolved maps of blood concentration and oxygenation in the capillary bed of skin tissue. Though microvascular oxygenation of hemoglobin may not be a direct measure of intracellular oxygen concentration, it does hold a strong correlation to it. This relation has been extensively studied and modeled [21,22,24]. The key distinction between the use of visible and near infrared wavelengths to characterize hemoglobin concentration lays with the characteristic depth these wavelength regimes interrogate in tissues such as skin. Scattering within bulk skin tissue is three to four times stronger in the visible wavelength regime than what is typically found in the near infrared. Similarly, absorption coefficient is nearly an order of magnitude stronger in the visible than in the near infrared. As a result, SFDI derived quantitative absorption values in the visible typically reflect chemical properties of the skin approximately within the first millimeter of tissue, whereas absorption coefficient values obtained based on near infrared wavelengths reflect the composition of volumes of tissue that lie deeper, within a few millimeters [27]. This differentiation in interrogation volumes by employing visible wavelengths versus near infrared wavelengths suggests that visible wavelengths can be used to report the blood oxygenation within the volume of tissue containing the lesion, the near infrared wavelengths can be used as an indicator for the blood oxygenation and supply beneath the lesion.

Visible wavelengths are also more greatly affected by the presence of epidermal melanin. Though NMSC is typically present in primarily fair skinned individuals, melanin may influence the total absorption of the light used to interrogate the tissue. Using both visible

and near infrared absorption values to fit for blood and melanin presents the opportunity to model tissue oxygenation with some depth resolution [27], but also isolate and remove the effect of melanin.

In addition to a large range of spatial variation in optical properties measured using this instrument, we also observed a large range of variation in optical properties between patients. Given that the range in variation here was similar to that measured in terms of the intra-patient spatial variation in optical properties; this initial finding indicates the potential impact that inter-subject variability could have on an uninformed PDT treatment regimen. The question remains as to whether this inter- and intra-subject variation, though relatively large, would have any significant impact on the outcome of PDT treatment. Since this system is designed to deliver controlled, spatially resolved light in order to measure the optical properties of skin, our system is also capable of determining and delivering controlled, spatially resolved treatment light dose.

To date, the SFDI instrument described here has been used to characterize the optical and physiological properties of BCC and SCC lesions prior to treatment. This has provided some initial insight into the performance of the instrument and the range of optical properties present within these lesions. In a separate study, we have also examined this instrument's ability to determine photosensitizer uptake and concentration through a quantitative fluorescence imaging approach [31]. However, PDT is a dynamic process. The next critical step to validate this instrument is the verification of its ability to detect dynamic changes in oxygenation and characterize the depletion and repletion rates of tissue oxygenation as well as optical properties of tissue and photosensitizer concentration during treatment. These steps are planned for the next phase of study.

CONCLUSION

An LED-based SFDI instrument has been designed with clinical deployment and accessibility in mind and has therefore incorporated consumer grade components, such as LED's to manage the overall instrument costs. Initial system performance indicates that this instrument is capable of determining optical properties of tissue that are relevant to modeling light transport of therapeutic light in affected tissues and the quantification of blood concentration and oxygenation in the dermal microvasculature. We have demonstrated that for superficial BCC and SCC measured *in vivo*, considerable spatial and inter-subject variation exists. Furthermore, local oxygen saturation for lesion and adjacent tissue has been determined using SFDI and the variations in depth distributed oxygen saturation can be assessed by comparing oxygenation results obtained at visible (<1 mm) and near infrared (>1 mm) wavelengths. As an aggregate, the information provided by SFDI has the potential to inform PDT treatment parameters, thereby providing more quantitative and controlled dosimetry specific to the lesion. Ultimately, by optimizing the execution of PDT, this instrument has the potential to positively improve treatment outcomes.

Acknowledgments

We acknowledge funding and support from U.S. Army Medical Research, Award #: W81XWH-08-1-0086, Apogen Technologies, Inc, San Diego, CA, NIH NIBIB Biomedical Technology Research Center (LAMMP: P41EB015890), and the Beckman Foundation.

References

1. Stern RS. Prevalence of a history of skin cancer in 2007 results of an incidence-based model. Arch Dermatol. 2010; 146:279–282. [PubMed: 20231498]

2. Jemec GB, Holm EA. Nonmelanoma skin cancer in organ transplant patients. Transplantation. 2003; 75:253–257. [PubMed: 12589142]
3. Schweiger ES, Kwasniak L, Tonkovic-Capin V. A patient with neviod basal cell carcinoma syndrome treated successfully with photodynamic therapy: Case report and review of the literature. J Drugs Dermatol. 2010; 9:167–168. [PubMed: 20214182]
4. Guleng GE, Helsing P. Photodynamic therapy for basal cell carcinomas in organ-transplant recipients. Clin Exp Dermatol. 2012; 37:367–369. [PubMed: 22420420]
5. Lee Y, Baron ED. Photodynamic therapy: Current evidence and applications in dermatology. Semin Cutan Med Surg. 2011; 30:199–209. [PubMed: 22123417]
6. Apalla Z, Sotiriou E, Chovarda E, Lefaki I, Devliotou-Panagiotidou D, Ioannides D. Skin cancer: Preventive photodynamic therapy in patients with face and scalp cancerization. A randomized placebo-controlled study. Br J Dermatol. 2010; 162:171–175. [PubMed: 19863513]
7. Braathen LR, Morton CA, Basset-Seguin N, Bissonnette R, Gerritsen MJ, Gilaberte Y, Calzavara-Pinton P, Sidoroff A, Wulf HC, Szeimies RM. Photodynamic therapy for skin field cancerization: An international consensus. International Society for Photodynamic Therapy in Dermatology. J Eur Acad Dermatol Venereol. 2012; 26:1063–1066. [PubMed: 22220503]
8. Kendall CA, Morton CA. Photodynamic therapy for the treatment of skin disease. Technol Cancer Res Treat. 2003; 2:283–288. [PubMed: 12892510]
9. Marcus SL, Sobel RS, Golub AL, Carroll RL, Lundahl SL, Shulman DG. Photodynamic therapy (PDT) and photodiagnosis (PD) using endogenous photosensitization induced by 5-aminolevulinic acid (ALA): Current clinical and development status. SPIE J Clin Lasers Surg Med. 1996; 14(2): 59–66.10.1089/clm.1996.14.59
10. Orenstein, A.; Kostenich, G.; Tsur, H.; Roitman, L.; Ehrenberg, B.; Malik, Z. Photodynamic therapy of human skin tumors using topical application of 5-aminolevulinic acid, dimethylsulfoxide (DMSO), and edetic acid disodium salt (EDTA). Proc. SPIE 2325, Photodynamic Therapy of Cancer II; January 12, 1995;
11. Schleier, P.; Zenk, W.; Hyckel, P.; Berndt, A. Comparison between mALA- and ALA-PDT in the treatment of basal cell carcinomas. Proc. SPIE 6139, Optical Methods for Tumor Treatment and Detection: Mechanisms and Techniques in Photodynamic Therapy XV; March 06, 2006;
12. Bath-Hextall F, Bong J, Perkins W, Williams H. Interventions for basal cell carcinoma of the skin: Systematic review. BMJ. 2004; 329:705. [PubMed: 15364703]
13. Cosgarea R, Susan M, Crisan M, Senila S. Photodynamic therapy using topical 5-aminolaevulinic acid vs. surgery for basal cell carcinoma. J Eur Acad Dermatol Venereol.
14. Morton CA. The emerging role of 5-ALA-PDT in dermatology: Is PDT superior to standard treatments? J Dermatolog Treat. 2002; 13:S25–S29. [PubMed: 12060514]
15. Ziolkowski P, Osiecka BJ, Oremek G, Siewinski M, Symonowicz K, Saleh Y, Bronowicz A. Enhancement of photodynamic therapy by use of aminolevulinic acid/glycolic acid drug mixture. J Exp Ther Oncol. 2004; 4:121–129. [PubMed: 15503395]
16. Baptista J, Martinez C, Leite L, Cochito M. Our PDT experience in the treatment of non-melanoma skin cancer over the last 7 years. J Eur Acad Dermatol Venereol. 2006; 20:693–697. [PubMed: 16836497]
17. Patterson MS, Wilson BC, Graff R. In vivo tests of the concept of photodynamic threshold dose in normal rat liver photosensitized by aluminum chlorosulphonated phthalocyanine. Photochem Photobiol. 1990; 51:343–349. [PubMed: 2356229]
18. Hopper C. Photodynamic therapy: A clinical reality in the treatment of cancer. Lancet Oncol. 2000; 1:212–219. [PubMed: 11905638]
19. Zhou X, Pogue BW, Chen B, Demidenko E, Joshi R, Hoopes J, Hasan T. Photosensitizer dosimetry controlled PDT treatment planning reduces inter-individual variability in response to PDT. In Proc of SPIE. 2006; 6139:61390P–1.
20. Jacques SL. Optics of light dosimetry for PDT in superficial lesions versus bulky tumors. Proc SPIE, Int Soc Opt Eng. 2002; 4612:59–68.
21. Foster TH, Gao L. Dosimetry in photodynamic therapy: Oxygen and the critical importance of capillary density. Radiat Res. 1992; 130:379–383. [PubMed: 1594766]

22. Wang HW, Putt ME, Emanuele MJ, Shin DB, Glatstein E, Yodh AG, Busch TM. Treatment-induced changes in tumor oxygenation predict photodynamic therapy outcome. Cancer Res. 2004; 64:7553–7561. [PubMed: 15492282]
23. Cottrell WJ, Paquette AD, Keymel KR, Foster TH, Oseroff AR. Irradiance-dependent photobleaching and pain in delta-aminolevulinic acid-photodynamic therapy of super-ficial basal cell carcinomas. Clin Cancer Res. 2008; 14:4475–4483. [PubMed: 18628462]
24. Wang KK, Cottrell WJ, Mitra S, Oseroff AR, Foster TH. Simulations of measured photobleaching kinetics in human basal cell carcinomas suggest blood flow reductions during ALA-PDT. Lasers Surg Med. 2009; 41:686–696. [PubMed: 19802891]
25. Cuccia DJ, Bevilacqua F, Durkin AJ, Tromberg BJ. Modulated imaging: Quantitative analysis and tomography of turbid media in the spatial-frequency domain. Opt Lett. 2005; 30:1354–1356. [PubMed: 15981531]
26. Mazhar A, Sharif SA, Cuccia JD, Nelson JS, Kelly KM, Durkin AJ. Spatial frequency domain imaging of port wine stain biochemical composition in response to laser therapy: A pilot study. Lasers Surg Med. 2012; 44:611–621. [PubMed: 22911574]
27. Saager RB, Truong A, Cuccia DJ, Durkin AJ. Method for depth-resolved quantitation of optical properties in layered media using spatially modulated quantitative spectroscopy. J Biomed Opt. 2011; 16:077002. [PubMed: 21806282]
28. Saager RB, Cuccia DJ, Durkin AJ. Determination of optical properties of turbid media spanning visible and near-infrared regimes via spatially modulated quantitative spectroscopy. J Biomed Opt. 2010; 15:017012. [PubMed: 20210486]
29. Mazhar A, Cuccia DJ, Gioux S, Durkin AJ, Frangioni JV, Tromberg BJ. Structured illumination enhances resolution and contrast in thick tissue fluorescence imaging. J Biomed Opt. 2010; 15:010506. [PubMed: 20210421]
30. Konecky SD, Owen CM, Rice T, Valdes PA, Kolste K, Wilson BC, Leblond F, Roberts DW, Paulsen KD, Tromberg BJ. Spatial frequency domain tomography of protoporphyrin IX fluorescence in preclinical glioma models. J Biomed Opt. 2012; 17:056008. [PubMed: 22612131]
31. Saager RB, Cuccia DJ, Saggese S, Kelly KM, Durkin AJ. Quantitative fluorescence imaging of protoporphyrin IX through determination of tissue optical properties in the spatial frequency domain. J Biomed Opt. 2011; 16:126013. [PubMed: 22191930]
32. Cuccia DJ, Bevilacqua F, Durkin AJ, Ayers FR, Tromberg BJ. Quantitation and mapping of tissue optical properties using modulated imaging. J Biomed Opt. 2009; 14:024012. [PubMed: 19405742]
33. Kienle A, Patterson MS. Improved solutions of the steady-state and the time-resolved diffusion equations for reflectance from a semi-infinite turbid medium. J Opt Soc Am A Opt Image Sci Vis. 1997; 14:246–254. [PubMed: 8988618]
34. Singer AJ, Clark RA. Cutaneous wound healing. N Engl J Med. 1999; 341:738–746. [PubMed: 10471461]
35. Kobayashi M, Ito Y, Sakauchi N, Oda I, Konishi I, Tsunazawa Y. Analysis of nonlinear relation for skin hemoglobin imaging. Opt Express. 2001; 9:802–812. [PubMed: 19424318]
36. Morton CA, MacKie RM, Whitehurst C, Moore JV, McColl JH. Photodynamic therapy for basal cell carcinoma: Effect of tumor thickness and duration of photosensitizer application on response. Arch Dermatol. 1998; 134:248–249. [PubMed: 9487227]
37. Busch TM, Xing X, Yu G, Yodh A, Wileyto EP, Wang HW, Durduran T, Zhu TC, Wang KK. Fluence rate-dependent intratumor heterogeneity in physiologic and cytotoxic responses to Photofrin photodynamic therapy. Photochem Photobiol Sci. 2009; 8:1683–1693. [PubMed: 20024165]
38. Carp SA, Prahl SA, Venugopalan V. Radiative transport in the delta-P1 approximation: Accuracy of fluence rate and optical penetration depth predictions in turbid semi-infinite media. J Biomed Opt. 2004; 9:632–647. [PubMed: 15189103]

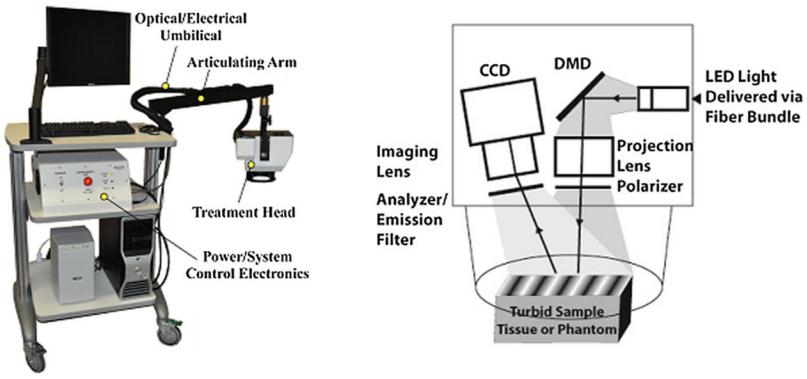

Fig. 1.
Image of clinical instrumentation and schematic of imaging/treatment head of the instrument.

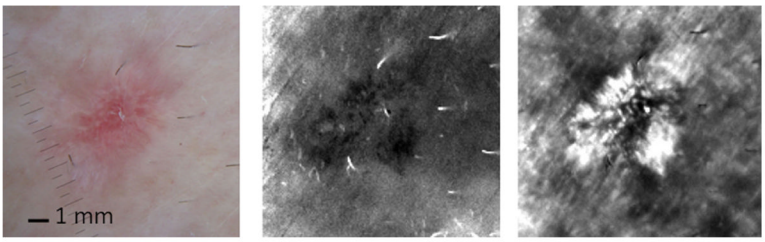

Fig. 2.

Left: Clinical photo of an example BCC lesion (subject 2), (**middle**) the determined absorption coefficient for that lesion (range: 0.042–0.002 mm^{-1}), and (**right**) the reduced scattering coefficient (range: 6.5–1.8 mm^{-1}). Scale bars are 1 mm and apply to all images.

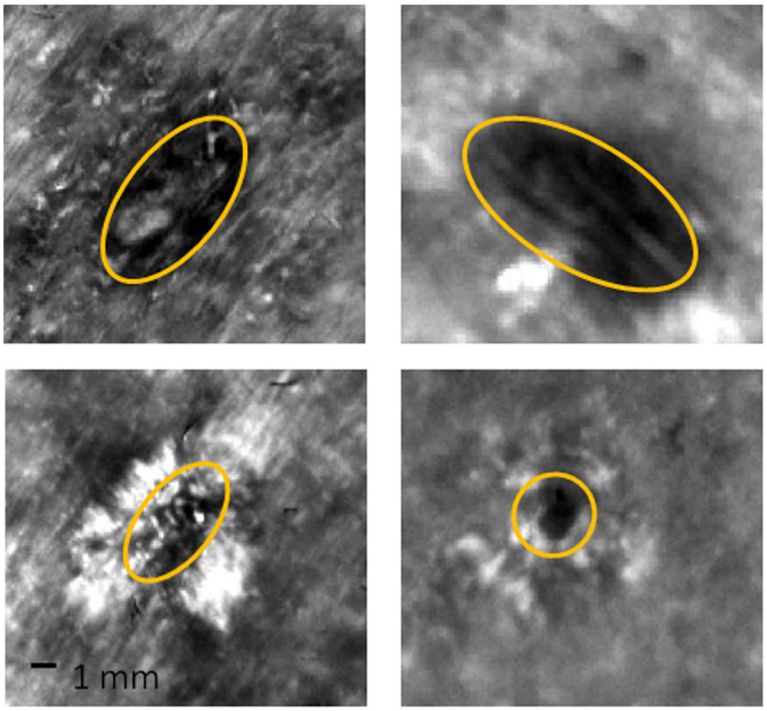

Fig. 3.

Spatially resolved reduced scattering coefficient (630 nm) of four different biopsied BCC lesions (from Table 1, Subjects 1a: **top left**, 1b: **top right**, 2: **bottom left**, and 8: **bottom right**). Ovals indicate the location of the biopsies. Nine weeks post-biopsy (**top row**), 2 and 4 weeks post-biopsy, respectively (**bottom row**). All images are shown in greyscale ranging 0.85–6.5 mm^{-1}. Scale bars are 1 mm and apply to all images.

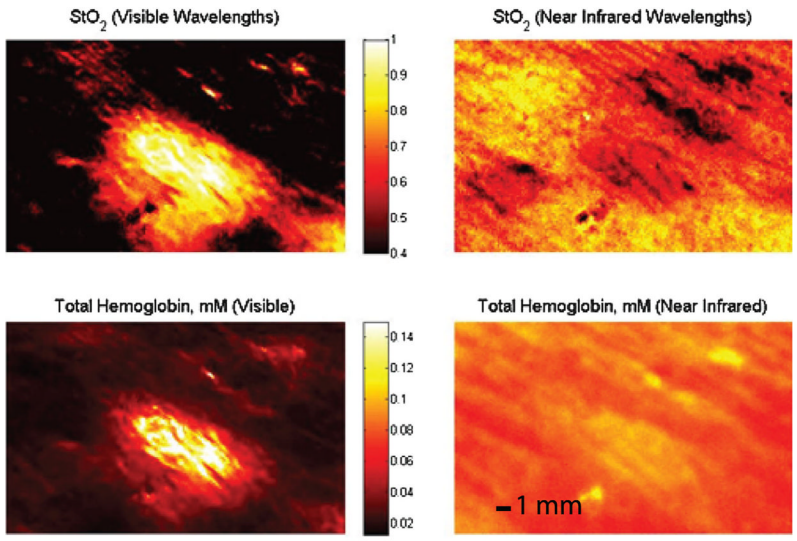

Fig. 4.

Visible (**left**) and Near Infrared (**right**) determination of tissue oxygenation, StO_2, (**top**) and total hemoglobin maps (**bottom**) a BCC lesion from subject 1(b). All images are scaled from fractional values of 0.4–1.0 (i.e., 40–100%) StO_2 (**top left** and **right**), and 0–0.150 mmol/ml hemoglobin concentration (**bottom left** and **right**), respectively. Scale bars are 1 mm and apply to all images.

TABLE 1

Summary of Subjects Imaged and Analyzed

	Imaged	Time from biopsy	Pathology	Location
Subject 1	Post-biopsy	9 weeks	Superficial BCC	Upper right back
	Post-biopsy	9 weeks	Superficial BCC	Upper left back
Subject 2	Post-biopsy	4 weeks	Superficial BCC	Lower left leg
Subject 3	Pre biopsy	n/a	Superficial BCC	Upper left arm
Subject 4	Pre biopsy	n/a	SCC *in situ*	Right forearm
Subject 5	Pre biopsy	n/a	SCC *in situ*	Left forearm
Subject 6	Pre biopsy	n/a	Superficial BCC	Upper left back
Subject 7	Pre biopsy	n/a	SCC *in situ*	Upper right back
Subject 8	Post-biopsy	2 weeks	Superficial BCC	Left forearm

TABLE 2

Average and Range of Optical Properties Measured at 630 nm

Subject	μ_a (mm^{-1})	Max/min	μ'_s (mm^{-1})	Max/min	Penetration depth (mm)
1a	0.047	0.123/0.019	1.69	2.54/1.06	2.02 (1.01/4.03)
1b	0.046	0.113/0.022	1.76	4.09/0.85	2.00 (0.84/4.17)
2	0.009	0.042/0.002	2.30	6.57/1.89	4.01 (1.10/9.36)
3	0.017	0.029/0.007	1.83	3.30/1.17	3.26 (1.86/6.36)
4	0.025	0.043/0.009	1.82	2.57/1.28	2.69 (1.72/5.36)
5	0.017	0.029/0.010	1.70	1.95/1.55	3.37 (2.41/4.62)
6	0.027	0.059/0.018	1.74	2.41/1.44	2.64 (1.51/3.56)
7	0.004	0.006/0.001	2.40	2.58/2.28	5.89 (4.64/12.1)
8	0.012	0.037/0.003	2.18	3.45/1.27	3.56 (1.61/9.34)

Here, μ_a refers to the absorption coefficient, μ_S the reduced scattering coefficient (red values indicate the range of reduced stattering coefficient from biopsied lesions).

TABLE 3

Results of Blood Concentration (Hb_{tot}) and Oxygenation (StO_2) for Normal Skin Versus NMSC

	Visible				Near infrared			
	Hb_{Tot} (lesion; μM)	**Hb_{Tot} (healthy tiss.; μM)**	**Penetration depth (mm)**	**StO_2 (lesion; %)**	**Hb_{Tot} (lesion; μM)**	**Hb_{Tot} (healthy tiss.; μM)**	**Penetration depth (mm)**	**StO_2 (%)**
Subject 1	35	9.6	1.2	80	107	106	5.75	76
	47	12	1.8	80	110	103	7.18	79
Subject 2	19	6.3	0.85	68	102	104	3.48	72
Subject 3	23	8.4	0.96	67	89	90	3.11	67
Subject 4	24	9.7	1.42	72	97	95	4.46	73
Subject 5	33	7.7	1.11	63	94	93	3.36	65
Subject 6	12	5.1	1.13	72	84	82	4.27	76
Subject 7	20	4.5	0.82	60	89	91	3.56	64
Subject 8	40	13	1.25	74	128	98	3.99	89